Polyhedron 62 (2013) 110–119

Contents lists available at SciVerse ScienceDirect

Polyhedron

journal homepage: www.elsevier.com/locate/poly

Synthesis, structure, spectroscopic properties, electrochemistry, and DFT correlative studies of *trans*-[Ru(P-P)$_2$Cl$_2$] complexes

Mousa Al-Noaimi [a,*], Ismail Warad [b,*], Obadah S. Abdel-Rahman [c], Firas F. Awwadi [d], Salim F. Haddad [d], Taibi B. Hadda [e]

[a] Department of Chemistry, Hashemite University, P.O. Box 150459, Zarqa 13115, Jordan
[b] Department of Chemistry, AN-Najah National University, Nablus, Occupied Palestinian Territory
[c] Fachbereich Chemie der Universität Konstanz, Universitätstraße 10, D-78457 Konstanz, Germany
[d] Chemistry Department, Faculty of Science, The University of Jordan, Amman 11942, Jordan
[e] Laboratoire LCM, Faculty of Sciences, University Mohammed 1er, Oujda 60000, Morocco

ARTICLE INFO

Article history:
Received 22 April 2013
Accepted 16 June 2013
Available online 27 June 2013

Keywords:
Ruthenium
Diphosphine
Electrochemistry
DFT calculation

ABSTRACT

Five *trans*-[Ru(P-P)$_2$Cl$_2$] complexes were prepared by reacting RuCl$_2$(PPh$_3$)$_3$ with P-P ligands {P-P = 3-hexyl-1,3-bis(diphenylphosphino)propane (hdppp) (**1**); = 1,3-bis(diphenylphosphino)propane (dppp) (**2**); = 1,2-bis(diphenylphosphino)ethane (dppe) (**3**); 1.1′-bis(diphenylphosphino)methane (dppm) (**4**); 1,2-bis(diphenylphosphino)ethylene (depe) (**5**)}. The complexes were characterized by an elemental analysis, IR, ^{1}H, ^{13}C and ^{31}P{1H}NMR, FAB-MS and TG/DTA. These Ru(II) complexes showed Ru(III)/Ru(II) quasireversible redox couple. The molecular structures of the complexes **1** and **3** were determined by X-ray crystallography, and their spectroscopic properties were studied. Another polymorph of **3** was reported in literature, the reported polymorph of **3** in this work crystallizes in $P\bar{1}$ space group, whereas, the previously reported polymorph crystallizes in *C*2/*c* space group. The two complexes adopt a distorted *trans* octahedral coordination and ruthenium(II) ions are located on a crystallographic centre of symmetry. Based on the optimized structures, computational investigations were carried out in order to determine the electronic structures of the complexes. The electronic spectra of **1** and **1**$^+$ in dichloromethane were calculated with the use of time-dependent DFT methods, and the electronic spectra of the transitions were correlated with the molecular orbitals of the complexes.

1. Introduction

Ruthenium(II) complexes with polydentade phosphines ligands have received much attention in the last decades due to their application in the field of homogeneous catalysis [1,2]. Several complexes of the general formula *cis*- and *trans*-[M(P-P)$_2$X$_2$] (P-P = C$_2$H$_4$(PR$_2$)$_2$ (R = Me, Et or Ph), CH$_2$(PPh$_2$)$_2$, and *o*-C$_6$H$_4$(PEt$_2$)$_2$; X = halogen, SCN^{-1}, H^{-1}, CN^{-1}) (M = Ru, Os) were prepared by Chatt and Hayter [3,4]. These complexes, *trans*-[Ru(P-P)$_2$Cl$_2$], could be used as starting materials to prepare bi- and pronuclear complexes [5,6]. Classical procedures for the syntheses of these complexes require the reflux conditions in acidic media [7] or the aqueous solution of K$_2$[RuCl$_5$(H$_2$O)] [8]. Poor yields of complexes are obtained by these preparation procedures. For this reason, a study of the electronic structures of such complexes is valuable as a mean to predict their properties [9–11].

In this paper, we present the synthesis, crystal, molecular, the electronic structures, and the spectroscopic characterization of five ruthenium(II) complexes with diphosphine ligands. The *trans*-[Ru(P-P)$_2$Cl$_2$] complexes, (P-P) {P-P = (Hdppp) = 3-hexyl-1,3-bis(diphenylphosphino)propane (**1**); (dppp) = 1,3-bis(diphenylphosphino)propane (**2**); (dppe) = 1,2-bis(diphenylphosphino)ethane (**3**) (dppe); (dppm) 1.1′-bis(diphenylphosphino)methane (**4**); 1,2-bis(diphenylphosphino)ethylene (**5**)}, were prepared from the reaction RuCl$_2$(PPh$_3$)$_3$ and the corresponding P-P ligand. These *trans* complexes have a poor solubility in many organic solvents. The solubility can be improved by modification of the diphospine backbone chelating ligand with alkyl group. Hdppp is a newly prepared diphosphine ligand to improve the solubility of the *trans*-[Ru(P-P)Cl$_2$] complexes. To probe the effect of the size of chelating ring of P-P on the electronic behavior *trans*-[RuCl$_2$(P-P)$_2$] complexes. In this work, we present and discuss the spectroscopic (IR, UV–Vis, ^{1}HNMR and ^{31}PNMR) and electrochemical (cyclic voltammetry) behavior of **1**–**5**, and report the X-ray structures for **1** and **3**. The absorption spectrum of complex **1** and **1**$^+$ in dichloromethane have been modeled by time-dependent density functional theory (TD-DFT) using a mixed basis set, MWB/6-31+g(d,p) to correlate experimental findings with theoretical predictions.

* Corresponding authors.
E-mail address: manoaimi@hu.edu.jo (M. Al-Noaimi).

0277-5387/$ - see front matter © 2013 Elsevier Ltd. All rights reserved.
http://dx.doi.org/10.1016/j.poly.2013.06.024

2. Experimental

2.1. Materials

The reagents: ruthenium trichloride hydrate, 1,3-bis(diphenylphosphino)propane (dppp), 1,2-bis(diphenylphosphino)ethane (dppe), 1.1′-bis(diphenylphosphino)methane (dppm); 1,2- cis-1,2-bis(diphenylphosphino)ethylene (depe), *n*-Butyllithium solution 1.6 M in hexane, Diphenylphosphine, and solvents (reagent grade) were purchased from Aldrich and were used as received, 1-chloro-2-(chloromethyl)octane was purchased from MolPort, Tetrabutylammonium hexafluorophosphate (TBAHF), purchased from Aldrich, was recrystallized twice from 1:1 ethanol/water solution and then vacuum dried at 110 °C. The synthesis of $RuCl_2(PPh_3)_3$ has been previously described [6].

2.2. Syntheses

2.2.1. Synthesis of 2-hexyl-1,3-bis(diphenylphosphino)propane (Hdppp) ligand

The new ligand was prepared following published procedures [12,13]. A solution of n-BuLi in *n*-hexane (25 mL of a 1.6 M solution, 2.56 g) was added dropwise to a solution of diphenylphosphine, Ph_2PH (7.44 g, 40.0 mmol) in dry THF (20 ml) at −5 °C over 5 h. The prepared red solution consisting of Ph_2PLi was stirred for 2 hours at ambient temperature. Then a solution of 1-chloro-2-(chloromethyl)octane (3.94 g, 20.0 mmol) in dry THF (20 mL) was added dropwise within 40 min until all the red color was disappeared. The reaction temperature was kept at 0 °C during the addition and the solution was stirred for another 4 h to ensure that the reaction went to completion. To the colorless mixture, a degassed aqueous solution saturated with NH_4Cl (100 mL) was added and the organic layer was separated. The solution was dried with Na_2SO_4 and separated from the solid residue. After the evaporation of the volatile materials under vacuum, the crude product was distilled to yield highly viscous colorless air sensitive oil. Yield (8.0 g, 81%). UV–Vis in dichloromethane: λ_{max} = 237 nm. ^{1}H NMR ($CDCl_3$): δ (ppm), 0.7 (br, 3H, 1C*H*$_3$), 1.0–2.1 (3 br, 11H, 5C*H*$_2$ and 1C*H*), 2.4 (m, 4H, 2PC*H*$_2$), 6.8–7.9 (3 m, *20H*, Phs). ^{31}P{^{1}H} NMR ($CDCl_3$): δ (ppm) −21.5. MS (EI): M^+ 496.2 (*m*/*z*). IR (KBr, cm^{-1}): 3180 (υ_{PhH}) and 2970 (υ_{CH}). 1520 ($\upsilon_{C=C}$). Elemental *Anal.* Calc. for $C_{33}H_{38}P_2$: C, 79.81; H, 7.71. Found: C, 79.63; H, 7.65%.

2.2.2. General procedure for the syntheses of trans-[Ru(P-P)$_2$Cl$_2$] (**1**–**5**) complexes

Diphosphine ligand (2.0 mmol) was dissolved in 10 mL of dichloromethane and the solution was added dropwise to a stirred solution of $RuCl_2(PPh_3)_3$ (1.0 mmol) in 10 mL of dichloromethane. The reaction mixture was stirred approximately for 50 min at room temperature. The brown solution was filtered to remove the insoluble impurities. The solvent was reduced by a vacuum and the product was then precipitated by adding *n*-hexane. The yellow solid was filtered and washed three times with 20 mL of diethyl ether.

*2.2.2.1. trans-[Ru(Hdppp)$_2$Cl$_2$] (**1**).* Yield (1.06 g, 91%). UV–Vis in dichloromethane: λ_{max}(nm) (ε_{max}, $M^{-1}\,cm^{-1}$): 465 (4.21×10^2), 365 (4.95×10^2), 340 (2.320×10^3). IR (KBr, cm^{-1}): 3160 (υ_{PhH}) and 2960 (υ_{CH}), 1520 ($\upsilon_{C=C}$), 450 (υ_{Ru-P}).^{1}H NMR ($CDCl_3$): δ (ppm), 0.6 (2 br, 6 H, 2 C*H*$_3$), 0.7–3.1 (4 br, 22 H, 10 C*H*$_2$ and 2 C*H*), 2.9 (m, 8 H, 4 PC*H*$_2$), 6.5 −7.8 (4 m, 20 H, PC_6H_5). ^{31}P{1H}($CDCl_3$): δ (ppm) 2.2. FAB-MS: M^+ 1165.3 (*m*/*z*). Elemental *Anal.* Calc. for $C_{66}H_{76}Cl_2P_4Ru$: C, 68.71; H, 7.61. Found: C, 68.83; H, 7.41%.

*2.2.2.2. trans-[Ru(dppp)$_2$Cl$_2$] (**2**).* Yield (0.86 g, 87%). UV–Vis in dichloromethane: λ_{max} (nm) (ε_{max}, $M^{-1}\,cm^{-1}$): 475 (3.88×10^2), 375 (4.75×10^2), 350 (2.097×10^3). IR (KBr, cm^{-1}): 3166 (υ_{PhH}) and 2964 (υ_{CH}), 1525 ($\upsilon_{C=C}$), 454(υ_{Ru-}). 2.7 (m, 12 H, PCH_2, PCH_2), 7.01 (t, 16 H, PC_6H_5), 7.19 (t, 8 H, PC_6H_5), 7.37 (d, 16 H, PC_6H_5), ^{31}P {1H}($CDCl_3$): δ (ppm), 5.1. FAB-MS; [M+] 996.7 (*m*/*z*) Elemental *Anal.* Calc. for $C_{54}H_{52}Cl_2P_4Ru$: C, 65.06; H, 5.26. Found: C, 65.22; H, 5.40%.

*2.2.2.3. trans-[Ru(dppe)$_2$Cl$_2$] (**3**).* Yield (0.87 g, 90%). UV–Vis in dichloromethane: λ_{max} (nm) (ε_{max}, $M^{-1}\,cm^{-1}$): 447 (1.70×10^2), 380 (3.4×10^2), 312 nm (2.7×10^4). IR (KBr, cm^{-1}): 3155 (υ_{PhH}) and 2957 (υ_{CH}), 1517 ($\upsilon_{C=C}$), 445 (υ_{Ru-P}). ^{1}H NMR ($CDCl_3$): δ (ppm) 7.02–7.22 (3 m, 28 H, PC_6H_5), 2.73 (m, 8 H, 4 CH_2), ^{31}P {1H}($CDCl_3$): δ (ppm) 44.9. FAB-MS; [M+] 968.8 (*m*/*z*). Elemental *Anal.* Calc. for $C_{52}H_{48}Cl_2P_4Ru$: C, 64.47; H, 4.99. Found: C, 64.56; H, 4.70%.

*2.2.2.4. trans-[Ru(dppm)$_2$Cl$_2$] (**4**).* Yield. (0.77 g, 82%). UV–Vis in dichloromethane: λ_{max} (nm) (ε_{max}, $M^{-1}\,cm^{-1}$): 483 (1.95×10^2), 429 (2.8×10^2), 320 (2.4×10^3). IR (KBr, cm^{-1}): 3150 (υ_{PhH}) and 2955 (υ_{CH}), 1525 ($\upsilon_{C=C}$), 455 (υ_{Ru-P}). ^{1}H NMR ($CDCl_3$): δ (ppm) 4.0 (m, 4 H, PCH_2), 7.01 (t, 16 H, PC_6H_5), 7.18 (t, 8 H, PC_6H_5), 7.41 (m, 16 H, PC_6H_5), ^{31}P{1H}($CDCl_3$): δ (ppm) −7.1. FAB-MS; [M+] 940.5 (*m*/*z*). Elemental *Anal.* Calc. for $C_{50}H_{44}Cl_2P_4Ru$: C, 63.84; H, 4.71. Found: C, 63.56; H, 4.50%.

*2.2.2.5. trans-[Ru(depe)$_2$Cl$_2$] (**5**).* Yield. (0.77 g, 82%). UV–Vis in dichloromethane: λ_{max} (nm) (ε_{max}, $M^{-1}\,cm^{-1}$): 400 (3.96×10^2), 350 (2.54×10^3). IR (KBr, cm^{-1}): 3155 (υ_{PhH}) and 2955 (υ_{CH}), 1517 ($\upsilon_{C=C}$), 447 (υ_{Ru-P}), 318 (υ_{Ru-Cl}). ^{1}H NMR ($CDCl_3$): δ (ppm) 6.80 (d, 4 H, PC*H*), 7.0–7.21 (3m, 20 H, PC_6H_5), ^{31}P {1H}($CDCl_3$): δ (ppm) 53.7 FAB-MS; [M+] 964.7 (*m*/*z*). Elemental *Anal.* Calc. for $C_{52}H_{44}Cl_2P_4Ru$: C, 64.74; H, 4.60. Found: C, 64.56; H, 4.40%.

2.3. Instrumentation

^{1}H NMR (400 MHz) and ^{31}P NMR (162 MHz) spectra were measured on a Bruker Avance III 400 spectrometer as $CDCl_3$ solutions at room temperature. All chemical shifts are reported in ppm downfield of TMS (1H) or 85% phosphoric acid (^{31}P) and referenced using the chemical shifts of residual solvent resonances. IR spectra were measured by FT-IR JASCO model 420. Elemental analyses were carried out on an Eurovector E.A.3000 instrument using copper sample-tubes. FAB-MS data were obtained on a Bruker IFS 48 FT-IR spectrometer and Finnigan 711A (8 kV), modified by AMD and reported as mass/charge (*m*/*z*), respectively. UV–Vis/NIR spectra were recorded on a TIDAS fiberorptic diode array spectrometer (combined MCS UV/NIR and PGS NIR instrumentation) from j & m in HELLMA quartz cuvettes with 0.1 cm optical path lengths. Electrochemical measurements were performed in dichloromethane (Aldrich, HPLC grade) using BAS CV-27. All electrochemical experiments were done in a home-built cylindrical vacuum-tight one-compartment cell. A spiral-shaped Pt wire and an Ag wire as the counter and thin pseudo-reference electrodes are sealed into glass capillaries via standard joints and fixed by Quickfit screws. A platinum electrode is introduced as the working electrode through the top central port via a Teflon screw cap with a suitable fitting. It is polished with first 1 μm and then 0.25 μm diamond pastes before measurements. The cell was attached to a conventional Schlenk line via a side arm equipped with a Teflon screw valve and allows experiments to be performed under argon atmosphere with approximately 5 mL of analyte solution. Tetrabutylammonium hexafurophosphate (0.1 M) was twice recrystallized and vacuum dried at 120 °C, and used as the supporting electrolyte. The temperature was controlled (at 25.0 ± 0.1 °C) by a Haake D8-G

refrigerator. Referencing was done with an addition of one crystal of decamethylferrocene (Cp^*_2Fe) as an internal standard to the analyte solution after all data of interest had been acquired. Representative sets of scans were repeated with the added standard. Final referencing was done against the ferrocene/ferrocenium ($Cp_2Fe^{0/+}$) couple with $E_{1/2}$ $Cp^*_2Fe^{0/+} = -542$ mV versus $Cp_2Fe^{0/+}$[14,15]. Spectroelectrochemistry of a representative complex **1** was performed by using an optically transparent thin layer electrochemistry (OTTLE) cell [16]. OTTLE cell was home-built and comprises a Pt working and counter electrode and a thin silver wire as a pseudo-reference electrode sandwiched between two CaF_2 windows of a conventional liquid IR cell. The working electrode is positioned in the center of the spectrometer beam. The potential was controlled by the same BAS CV-27 that was used for cyclic voltammetry. At any given potential, the system was allowed to come to equilibrium (i ~0 A) before the spectrum was taken.

2.4. X-ray crystallography

Crystals were grown by a slow diffusion of diethyl ether into a solution of the complex in dichloromethane. Suitable yellow prismatic crystal of complexes **1** and **3** were mounted with epoxy on glass fiber and the data collected at room temperature employing Mo radiation, $\lambda = 0.71073$ Å and Bruker P4 diffractometer. For complex **1** cell measurements were based on 36 reflections between theta 4.5° and 15.0°, while for complex **3** on 66 reflections between 4.8° and 12.7°. Data was collected by ω scans. Two standard reflections recorded after each 98 counts showed no decay. Data collection and empirical absorption correction were performed by XSCANS [17] and data reduction by SHELXTL [18]. SHELXS [18] was used for structure solution and SHELXL [18] for structure refinement. Details of data collection and refinement are given in Table 1. Molecular graphics and publication material were generated using SHELXTL package.

The structure for complex **1** was solved by direct methods as $P2(1)/n$ and refined by least squares on F^2 to $R_1 = 0.0503$ [$I \geqslant 2\sigma(I)$] with $\theta = 2.02°$ to 27.50°. Goodness-of-fit on $F^2 = 1.021$. All nonhydrogen atoms were refined anisotropically except the six C atoms in the central part of the 2-methyloctane bridging moiety. The thermal parameters for these atoms are very high and anisotropic refinement generates some short bond distances. The hydrogen atoms, other than H14 and H63, were positioned constrained and assigned isotropic thermal parameters of 1.2 times that of the riding atoms. (1.5 times for methyl hydrogen atoms). H14 and H63 were located in a difference Fourier map and refined fully, for otherwise the data did not converge. Largest diffraction peak and hole were 1.865 and −0.73 e Å^{-3}. There are two independent half molecules in the asymmetric unit, one containing Ru1 and the other Ru2. ORTEP diagram [19] showing the numbering scheme are for the Ru1 molecule (Fig. 1).

The structure for complex **3** was solved by direct methods as $P\bar{1}$ and refined by least squares on F^2 to $R_1 = 0.0503$ [$I \geqslant 2\sigma(I)$] with $\theta = 2.10$–27.50°. Goodness-of-fit on $F^2 = 1.027$. All nonhydrogen atoms were refined anisotropically. The hydrogen atoms were located on the calculated positions using riding model and assigned isotropic thermal parameters of 1.2 times that of the riding atoms except methyl hydrogen atoms (1.5 times). The H atoms on C of the dichloromethane solvent were not locatable in a difference Fourier map, nor was it possible to position them due to the proximity of the C atom of the solvent, with 0.5 occupancy, at x, y, z with the symmetry related one at $1 - x$, $1 - y$, $-z$. Largest differaction peak and hole are 0.996 and −1.111 e Å^{-3}. Fig. 2 is an ORTEP diagram showing the numbering scheme in the molecular unit made from two inversions related asymmetric units. Selected bond distances and angles for both complexes **1** and **3** are listed in Table 2.

Table 1
Crystal data and structure refinement for complex **1** and **3**.

Complex	**1**	**3**
Empirical formula	$C_{66}H_{76}Cl_2P_4Ru$	$C_{53}H_{50}Cl_4P_4Ru_1$
Formula weight	1165.12	1053.68
T (K)	293(2)	298(2)
Wavelength (Å)	0.71073	0.71073
Crystal system	monoclinic	triclinic
Space group	$P2(1)/n$	$P\bar{1}$
Unit cell dimensions		
a (Å)	13.909(2)	10.0823(12)
b (Å)	22.443(3)	10.4860(9)
c (Å)	18.705(2)	13.0002(13)
α (°)	90	68.263(9)
β (°)	91.095(11)	70.648(13)
γ (°)	90	88.262(14)
V (Å^3)	5837.9(13)	1197.8(2)
Z	4	1
D_{calc} (Mg/m^3)	1.326	1.461
Absorption coefficient (mm^{-1})	0.510	0.721
$F(000)$	2440	540
Crystal size (mm^3)	0. 0.6 × 0.4 × 0.4	0.3 × 0.3 × 0.2
θ (°)	2.02–27.50	2.10–27.50
Index ranges	$-1 \leqslant h \leqslant 18$, $-29 \leqslant k \leqslant 1$, $-24 \leqslant l \leqslant 24$	$-13 \leqslant h \leqslant 13$, $-12 \leqslant k \leqslant 12$, $-16 \leqslant l \leqslant 16$
Reflections collected	15755	10734
Independent reflections (R_{int})	13368 (0.0214)	5368 (0.0210)
Completeness to theta = 27.50° (%)	99.8	97.5
Maximum and minimum transmission	0.3437 and 0.3163	0.5339 and 0.4951
Refinement method	full-matrix least-squares on F^2	full-matrix least-squares on F^2
Data/restraints/parameters	13368/0/612	5368/2/287
Goodness-of-fit (GOF) on F^2	1.021	1.027
Final R indices [$I > 2\sigma(I)$]	$R_1 = 0.0503$, $wR_2 = 0.1284$	$R_1 = 0.0333$, $wR_2 = 0.0893$
R indices (all data)	$R_1 = 0.0645$, $wR_2 = 0.1383$	$R_1 = 0.0364$, $wR_2 = 0.0922$
Largest difference in peak and hole (e Å^{-3})	1.865 and −0.731	0.996 and −1.111

$R_1 = \sum||F_o| - |F_c||/\Sigma|F_o|$; $wR_2 = \{\sum[\ w(F_o^2 - F_c^2)^2]/\sum[w(F_o^2)^2]\}^{1/2}$.

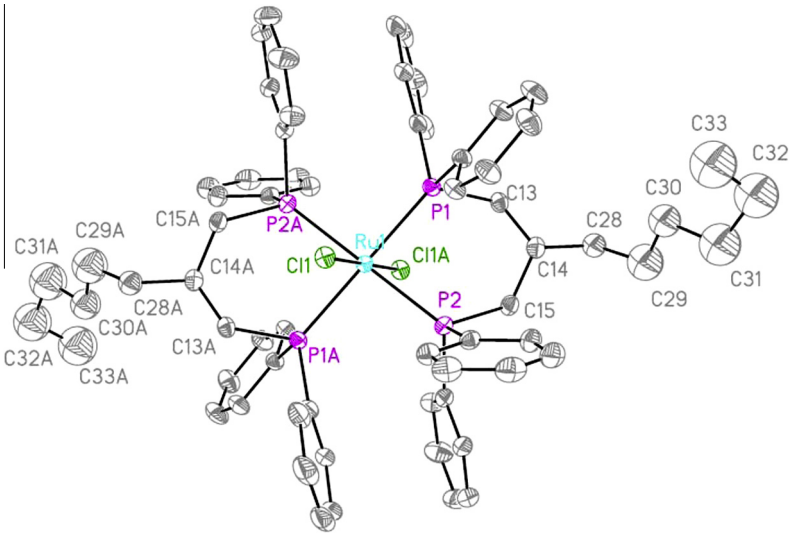

Fig. 1. Thermal ellipsoid drawing (30%) of complex **1**.

2.5. Computational methods

Full geometry optimization of **1** was carried out using density functional theory (DFT) at the B3LYP level [20]. All calculations were carried out using the GAUSSIAN 03 program package [21] with the aid of the GaussView visualization program [22]. For C, H, Cl and P the 6-31G(d) basis set were assigned, while for Ru, the MWB basis set with effective core potential were employed [23]. Vertical electronic excitations based on B3LYP optimized geometries were computed using the time-dependent density functional theory (TD-DFT) formalism [24–27] in dichloromethane using conductor-like polarizable continuum model (CPCM) [25]. Gauss Sum was used to calculate the fractional contributions of various groups to each molecular orbital [28].

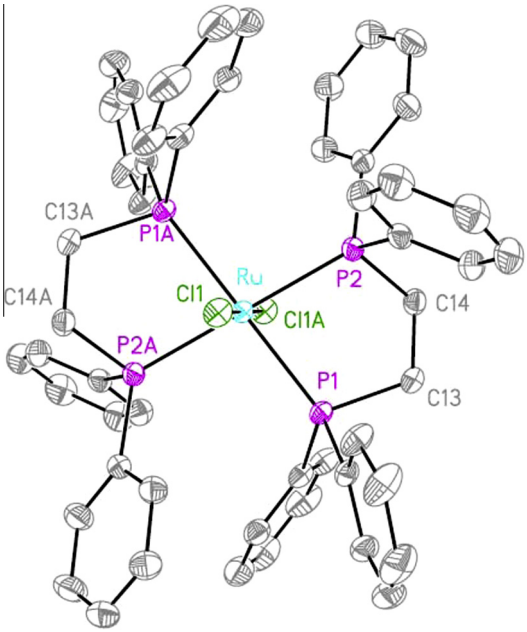

Fig. 2. Thermal ellipsoid drawing (30%) of complex **3**, solvent dichlormethane remove for clarity.

3. Results and discussion

3.1. Synthesis

The reaction scheme for the synthesis of ruthenium (II) complexes is depicted in Scheme 1. The yellow complexes of the formula *trans*-[Ru(P-P)$_2$Cl$_2$] (**1–5**) were obtained in a good yield by a substitution reaction of starting complex Ru(PPh)$_3$Cl$_2$ with two equivalent mole of P-P ligands in dichloromethane. For complex **1**, both up-up and up-down of the alkyl chain on the propyl of the Hdppp ligand can give two possible isomers. ^{1}H, ^{31}P n.m.r. spectra and X-ray structure confirm that there is only one product. thus we suggest that this complex is a more stable up-down alkyl chain isomer.

The structure of the desired complexes has been deduced from elemental analysis, infrared spectroscopy, FAB-mass spectrometry, ^{1}H, and ^{31}P n.m.r. spectra, TG/DTA spectroscopy. Additionally, the crystal structures of the complexes **1** and **3** were determined by X-ray crystallography. The ^{1}H NMR spectra of complexes **1–5** have been recorded in $CDCl_3$ solution to confirm the binding of the ligands to ruthenium and their assignments are given in Section 2.1. The ^{1}H NMR spectra of all the complexes present a set of signals in the region 7.0–7.2 and 1.7–3.3 ppm attributed to aromatic and aliphatic protons, respectively. The integration of the ^{1}H resonances confirms that the P-P ratio is in agreement with the structural composition of *trans*-[Ru(P-P)$_2$Cl$_2$] (**1–5**) complexes.

The ^{31}P n.m.r. spectra of these complexes (in $CDCl_3$) show one resonance; the obvious implication is that the four P atoms of each P-P are equivalent and the complexes are in octahedral geomety with *trans*-chloro ligands and non-exchanging phosphorus nuclei [29]. There are significant differences in the phosphorus chemical shifts between the complexes *trans*-[Ru(P-P)$_2$Cl$_2$] (**1–5**), which contains a five-membered chelate ring (complexes **3** and **5**), and those based on four (complex **4)** and six-membered chelate rings (complexes **1** and **2**). In the four-membered chelate complex the phosphorus resonates at lowest field, whereas the resonances of five-membered rings are observed at highest field (Table 3). The signals of six-membered rings (**1–2**) are positioned in between these two extremes, with that of slightly at higher field compared to that of four-member ring. Table 3 shows the Millikan charge for the phosphorus atom in addition the shift of the ^{31}P n.m.r. Millikan charges for phosphorus atom can be obtained from the DFT theoretical calculation (*vide infra*) and can be used as an indication

Table 2
Selected bond length (Å) and bond angles (°) for complex **1** and **3**.

Complex **1**				Complex **3**	
Molecule (Ru1) Bond angles (°) (experimental, optimized)		Molecule (Ru2) Bond lengths (Å)		Bond lengths (Å)	
Ru(1)–P(1A)	2.4182(9), 2.45159	Ru(2)–P(3)	2.4224(8)	Ru1–P(2)	2.3597(6)
Ru(1)–P(1)	2.4182(9), 2.45104	Ru(2)–P(3A)	2.4224(8)	Ru1–P(2A)	2.3597(6)
Ru(1)–P(2)	2.4212(8), 2.47365	Ru(2)–P(4A)	2.4303(8)	Ru1–P(1A)	2.3889(6)
Ru(1)–P(2A)	2.4212(8), 2.48146	Ru(2)–P(4)	2.4303(8)	Ru1–P(1)	2.3889(6)
Ru(1)–Cl(1A)	2.4377(8), 2.22869	Ru(2)–Cl(2)	2.4339(8)	Ru1–Cl(1)	2.4288(6)
Ru(1)–Cl(1)	2.4377(8), 2.23117	Ru(2)–Cl(2A)	2.4339(8)	Ru1–Cl(1A)	2.4288(6)
Bond angles (°) (experimental, optimized)		Bond angles (°)		Bond angles (°)	
P(1A)–Ru(1)–P(1)	180.0, 178.456	P(3)–Ru(2)–P(3A)	180.0	P(2)–Ru1–P(2A)	180.0
P(1A)–Ru(1)–P(2)	94.05(3), 93.652	P(3)–Ru(2)–P(4A)	92.99(3)	P(2)–Ru1–P(1A)	98.00(2)
P(1)–Ru(1)–P(2)	85.95(3), 84.659	P(3A)–Ru(2)–P(4A)	87.01(3)	P(2A)–Ru1–P(1A)	82.00(2)
P(1A)–Ru(1)–P(2A)	85.95(3), 84.698	P(3)–Ru(2)–P(4)	87.01(3)	P(2)–Ru1–P(1)	82.00(2)
P(1)–Ru(1)–P(2A)	94.05(3), 95.653	P(3A)–Ru(2)–P(4)	92.99(3)	P(2A)–Ru1–P(1)	98.00(2)
P(2)–Ru(1)–P(2A)	180.0, 179.658	P(4A)–Ru(2)–P(4)	180.0	P(1A)–Ru1–P(1)	180.0
P(1A)–Ru(1)–Cl(1A)	97.73(3), 96.486	P(3)–Ru(2)–Cl(2)	83.93(3)	P(2)–Ru1–Cl(1)	94.92(3)
P(1)–Ru(1)–Cl(1A)	82.27(3), 81.368	P(3A)–Ru(2)–Cl(2)	96.07(3)	P(2A)–Ru1–Cl(1)	85.08(3)
P(2)–Ru(1)–Cl(1A)	84.15(3), 83.659	P(4A)–Ru(2)–Cl(2)	97.50(3)	P(1A)–Ru1–Cl(1)	82.88(2)
P(2A)–Ru(1)–Cl(1A)	95.85(3), 96.068	P(4)–Ru(2)–Cl(2)	82.50(3)	P(1)–Ru1–Cl(1)	97.12(2)
P(1A)–Ru(1)–Cl(1)	82.27(3), 81.658	P(3)–Ru(2)–Cl(2A)	96.07(3)	P(2)–Ru1–Cl(1A)	85.08(3)
P(1)–Ru(1)–Cl(1)	97.73(3), 96.658	P(3A)–Ru(2)–Cl(2A)	83.93(3)	P(2A)–Ru1–Cl(1A)	94.92(3)
P(2)–Ru(1)–Cl(1)	95.85(3), 94.859	P(4A)–Ru(2)–Cl(2A)	82.50(3)	P(1A)–Ru1–Cl(1A)	97.12(2)
P(2A)–Ru(1)–Cl(1)	84.15(3), 83.598	P(4)–Ru(2)–Cl(2A)	97.50(3)	P(1)–Ru1–Cl(1A)	82.88(2)
Cl(1A)–Ru(1)–Cl(1)	180.0, 179.258	Cl(2)–Ru(2)–Cl(2A)	180.0	Cl(1)–Ru1–Cl(1A)	180.00(3)

for the shielding and the power of the σ-donation of the phosphorus atom. The calculated negative charges on the ruthenium and positive charges in phosphorus atoms which are obtained from natural population analysis are shown in Table 3. The negative charge on ruthenium is a result from the charge donation from the P-P and chloride ligands to the metal center. Also, the more positively charged phosphorus atom the more deshielded it is. So the phosphorous atoms of complex **4** with a four-membered ring is shielded more than six and five-membered rings. Similar data are to hand for complexes of Pd chromium, molybdenum and tungsten [30,31]. The double bond between the two P-P atoms in the five-membered ring (depe) makes the phosphorus atoms more deshielded compared to dppe and appears at 53.8 ppm for **5**. A similar effect has been observed in the series $[Pd(S_2CNEt_2)(P\text{-}P)]^+$ [32], *trans*-$[RuCl_2(P\text{-}P)_2]$ [7] and *fac*-$[RuCl_3(NO)(P\text{-}P)]$ [33].

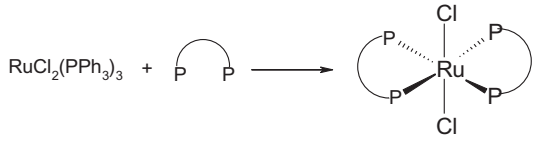

P-P ligand	Hdppp	dppp	dppe	dpppm	depe
Complex	**1**	**2**	**3**	**4**	**5**

Scheme 1.

Table 3
Cyclic Voltammetry[a], Electronic spectroscopy, $^{31}P\{1H\}$ and Millikan charge for *trans*-$[Ru(P\text{-}P)_2Cl_2]$(**1–5**).

Complexes	($E^\circ_{1/2}$, V) [b]	λ_{max} (nm)[a]	$^{31}P\{1H\}(CDCl_3)$	Millikan charge (Ru, P)
1	0.29	465, 425, 330	2.2	(−1.06, 0.66)
2	0.30	475, 375, 340	−5.1	(−1.03, 0.66)
3	0.37	447, 429,320	44.9	(−1.10, 0.70)
4	0.02	483, 429, 320	−7.1	(−1.13, 0.644)
5	0.45	445, 350	29.0	(−1.31, 0.710)

[a] Solvent dichloromethane.
[b] In volts vs. ferrocenium/ferrocene at 25 °C and scan rate of 0.1 V/s, 0.1 M TBAHF electrolyte.

Further strong evidence for the structural elucidation comes from FAB-MS spectra. For example, complex **1** shows a molecular ion peak [M+] m/z = 1165.3 which is corresponding to its molecular formula $[C_{66}H_{76}Cl_2P_4Ru]^+$ parent ion. The other fragments appeared in the spectrum are as m/z = 667 for $([C_{33}H_{38}P_2Cl_2Ru]^+$ and m/z = 597 $[C_{33}H_{38}P_2Ru]^+$.

The thermal decomposition studies of the **1-5** complexes were investigated in the 25–800 °C temperature range under open atmosphere at a heating rate of 10 °C/min. All the **1–5** complexes undergo one step decomposition with weight loss experimentally 86%, the coordinated chlorides, and P-P ligands have been moved away from the complex in between 260 and 400 °C with exothermic DTA peaks at 276.85 °C. The final residue was analyzed by IR spectra and identified as ruthenium oxide (RuO).

3.2. Crystal structures

The ruthenium atoms in the two complexes **1**, **3** (Figs. 1 and 2) are coordinated in a distorted octahedral with two chloride and two diphosphine (P-P) ligands are in a *trans* form and sited on a crystallographic centre of inversion. The asymmetric unit of **1** consisted of two halves of crystallographically different molecules. Other structures *trans*-$[Ru(dppm)_2Cl_2]$(C1) [34] and *trans*-$[Ru(dppp)_2Cl_2]$ (C2) [35] have been described in literature. In all structures the Ru–Cl distances are very similar: 2.426(1) in (Cl), 2.435(1) in (C2) and 2.426(1) in 2.436 (8) Å in the complex **1** and 2.4288 (6) for complex **3**. It is noticeable that structures of all the diphosphine complexes are symmetric, the Ru–P bond distances are 2.354(1) in (Cl), 2.4197(9) in C2 and 2.429(1) Å in C2 while the corresponding Ru-P bond distances are 2.3743(6) for **1** and 2.3743(6) for complex **3**. As expected, the Ru–P bond distances are directly proportionally to the length of the hydrocarbon chain between the diphosphines, due to the steric constraints imposed by the linkage on the conformation of the bidentate ligand.

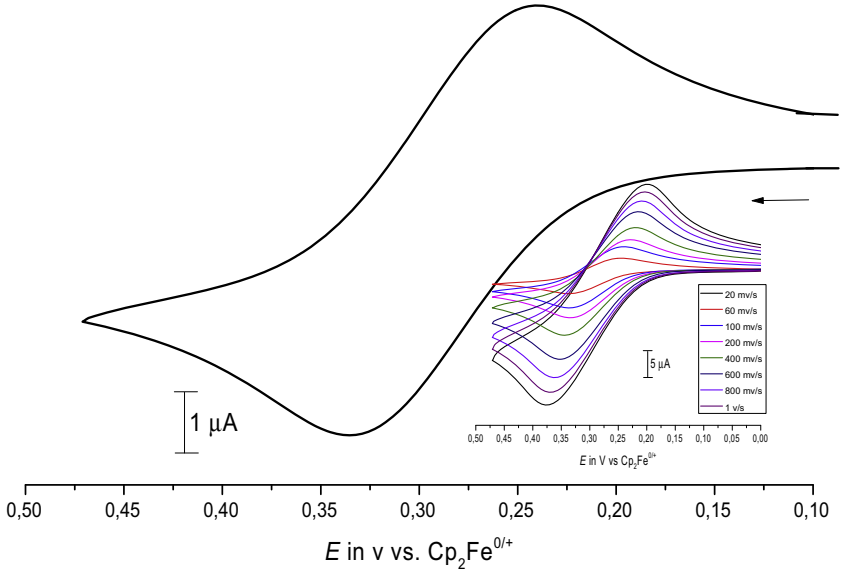

Fig. 3. Cyclic voltammogram for complex **1** in dichloromethane 0.1 M TBAH at 25 °C, data reported in V vs. ferocine with scan rate of 0.1 V/s, inset shows.

A different polymorph of *trans*-[Ru(dppe)$_2$Cl$_2$] (**3**) was prepared previously and was crystallized in *C*2/*c* group [36], whereas, the reported polymorph in this paper is crystallized in $P\bar{1}$ space group. Both phases are solvates, with disordered dichlorometane, the C2/c phase was grown by a slow evaporation of CH_2Cl_2, while, $P\bar{1}$ was grown by a slow diffusion of diethyl ether into a solution of the complex in dichloromethane (*vide supra*). According to the density rule the $P\bar{1}$ phase is the thermodynamically stable one; densities of the two polymorphs are 1.461 and 1.411 Mg/m^3 for $P\bar{1}$ and C2/*c* phases, respectively. The difference in the asymmetric units of the two polymorphs is minimal, excluding the dichloromethane molecule. However, the supramolecular structure of the two polymorphs differs significantly. The C9–H···Cl1 non-classical hydrogen bonding interactions connect the molecular units to form linear chains run parallel to *a*-axis. Hydrogen bonding parameters are 2.894, 3.599 Å and 133.64° for H···Cl1, C9···Cl1 and C9–H···Cl1, respectively. Selected bond distances and angles are given in Table 2.

For complex **1** (Fig. 1), the Cl–Ru–Cl angle is linear and the P–Ru–P angle of the chelate ring is 85.95(3) for Ru1 and 87.01(3) for Ru2. The coordination angle P–Ru–P angles of the chelate ring is 85.95(3)° for Ru1 and 87.01(3)° for Ru2 with negligible deviation from ideality due to seven-membered dppb chelate. For both complexes the plane of the phosphorus atoms are not perpendicular to the Cl–Ru–Cl. For example, Ru1 in complex **1**, the angles Cl(l)–Ru–P(1) and Cl(l)–Ru–P(2) have two different values (97.73(3), 95.85(3)) which means that the pseudo plane made by P(l)–P(2)–P(lA)–P(2A) is not perpendicular to the Cl–Ru–Cl axis.

In *trans*-[RuCl$_2$(dppm)$_2$] [34], the *trans* P–Ru–P angle is 71.4°. This angle is well-compared with the P–Ru–P angle for the complexes **1** and **3** in the present study. The P–Ru–P cone angle is 83.98°, 82.00(2)° for complexes **1** and **3**, respectively. In cases of dppm acting as a bidentate ligand coordinated to a single metal ion, contraction of the tetrahedral angle of the methylene carbon connecting the two phosphorus atoms occurs.

3.3. Electrochemistry

The electron-transfer behaviour of the complexes in dichloromethane solution was examined by cyclic voltammetry and the corresponding results are summarized in Table 3. The $E°_{1/2}$, values for the reversible couples were calculated from half the difference between $E°_{1/2}$ values for the anodic and cathodic waves from cyclic voltammetry. Decamethylferrocene was added as an internal standard near the end of the experiment[1]. The analyte potential was referenced to a ferrocene by subtracting 0.62 V [37]. This value can then be referenced to the NHE by adding 0.66 V [38]. As a representative example, the cyclic voltammogram for complex **1** is shown in Fig. 3. A one electron oxidation quasi reversible wave is observed at 0.29 V versus $Fc^{0/-}$. This wave is assigned to Ru(III/II) couple. This couple was quasi reversible with an anodic to cathodic peak separation of 80 mV. This separation was generally variant at scan rates from 20 to 1000 mV/s (inset Fig. 3).

Consequently, the less stable complex is easier to oxidize. There are significant differences in the $E°_{1/2}$ between the complexes Ru(P-P)$_2$Cl$_2$, which contain a five-membered chelate ring (complexes **3** and **4**) and those based on six-membered chelate rings (complexes **1** and **2**). In the four-membered chelate (complex **4)** the Ru(II) oxidized at lower potential, whereas the Ru (III/II) of five-membered rings (complex **3** and **5**) are observed at a highest potential (Table 3, Fig. 3). The Ru (III/II) of six-membered rings (complexes **1** and **2**) is positioned in between the four and five-membered rings. Adding a double bond to the dppe ligand (complex **3**) to generate depe (complex **5**) expected to increases the rigidity and the electronic delocalization between the two phosphorous atoms. These two factors stabilize the ruthenium center and thus increase its redox potential. A similar behaviour was observed for the [Ru(Cp)(P-P)(NO$_2$)] series, P-P = dppe, dppm or dmpe [39] on which the ruthenium (III/II) shifted to more anodic potentials when the more stable complex (P-P = dppe, dppm) is replaced with less stable [Ru(Cp)(dmpe)(NO$_2$)] complex [40].

3.4. UV–Vis and spectroelectrochemical studies

UV–Vis electronic absorption spectra of all the complexes were measured in dichloromethane. The changes in λ_{max} values based on a change of the phosphine ligand are tabulated in Table 3. The electronic absorption spectra of the *trans*-[Ru(P-P)$_2$Cl$_2$] (**1**–**5**) complexes are very similar, all have two weak absorption bands around 483–400 nm with a molar absorption coefficient of the order of 10^2 M^{-1} cm^{-1}, and an intense high energy absorption

[1] The ferrocene potential was too close to that of Ru(III/II) so decamethylferrocene was used as the internal standard.

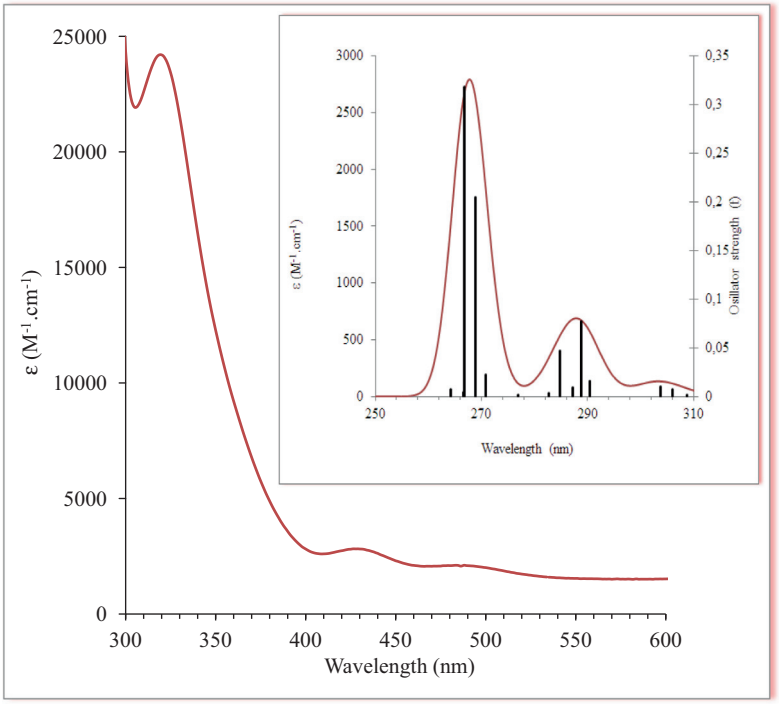

Fig. 4. UV-Vis. spectrum for **1** in dichloromethane. Inset shows simulated absorption spectrum. (black line) based on TD-DFT calculations, compared to excitation energies and oscillator strengths.

around 300–290 nm. Complex **1** as a representative example (Fig. 4) has three bands, two weak transitions around λ = 547 and 375 nm and a strong transition around 326 nm.

The electronic transitions for complex **1** in dichloromethane have been assigned based on the DFT and TDDFT calculation. Since the two molecules of complex **1** exhibit similar bond lengths and angles (Table 2), and for the sake of simplicity, molecule 1 was used for the present calculations. DFT calculation has been performed for the complexes **1** and $\mathbf{1}^{+}$. The optimized structure of this molecule is developed using GAUSSIAN 03 analyses package. The structural agreement has been observed from the comparison of bond distances and angles between calculated and X-ray determined structure (Table 2). The DFT calculated values for the bond angles were in closest agreement. The orbital energies along with contributions from the ligands and metal are given in Table 4 which depicts selected occupied and unoccupied frontier orbitals. Moreover, the isodensity plots for the HOMOs and LUMOs orbitals for complex **1** are shown in Fig. 5. The HOMO and HOMO−1 is constituted by >70% contribution from Ru where is HOMO−3 to HOMO−10 are mainly chloride in character. The LUMO is composed of 48% Ru and 38% of diphosphine ligand. This large contbution from the metal d-orbital in the LUMO suggests a significant back donation [41] from the Ru(dπ) → P(dπ)). LUMO+ is composed from 24% from Ru and 76% from diphosphine ligand. LUMO+2 to LUMO+10 are composed mainly from diphosphine ligands. The full theoretical absorption spectra were obtained from the calculation of the singlet excited states with TD-DFT at the B3LYP/MWB/6-31+g(d,p) level in the dichloromethane solution. Computation of 40 excited states of complex **1** allowed the interpretation of the experimental spectra in the 300–800 nm range (Fig. 4). The calculated energy of excitation states and transition oscillator strength (*f*) are shown in Table 5. The absorption spectrum of **1** was simulated using Gaussian Sum software [28] based on the obtained TD-DFT results. Each excited state was interpolated by a Gaussian convolution with the full width at half-maximum (fwhm) of 3000 cm^{-1}. Both the experimental UV–Vis spectrum of complex **1** reported in dichloromethane and its simulated absorption spectrum shown in Fig. 6 were in acceptable agreement. On the basis of its intensity and position, a weak broad band at 465 nm and 425, nm (≈303 and 288 nm (calculated)) resulted from HOMO → LUMO+1 (96%) and HOMO−2, HOMO− → LUMO thus band is assigned to d–d t_2(Ru) → e(Ru) transition [41]. The bands

Table 4
DFT energies and composition of selected highest occupied and lowest unoccupied molecular orbitals of complex **1** and $\mathbf{1}^{+}$ expressed in terms of composing fragments.

Complex	MO	E(eV)	Ru	Hdppp	Cl
1	L+5	−0.47	5	0	95
	L+4	−0.52	0	0	100
	L+3	−0.59	4	1	95
	L+2	−0.67	0	0	100
	L+1	−0.90	24	0	76
	L	−1.06	48	14	38
	H	−5.18	70	25	5
	H−1	−5.22	70	25	5
	H−2	5.91	81	0	19
	H−3	−6.18	2	14	84
	H−4	−6.2	3	19	78
	H−5	−6.51	2	0	97
$\mathbf{1}^{+}$	α MO				
	L+3	−1.16	3	97	0
	L+2	−1.23	0	100	0
	L+1	−2.33	34	66	0
	L	−3.23	49	23	27
	H	−6.86	2	97	1
	H−1	−7.02	2	97	1
	H−2	−7.02	4	94	2
	H−3	−7.08	0	98	0
	β MO				
	L+3	−1.23	3	97	0
	L+2	−2.09	0	100	0
	L+1	−2.93	36	64	0
	L	−4.84	52	24	24
	H	−6.87	77	6	17
	H−1	−6.98	2	97	1
	H−2	−7.01	44	28	28
	H−3	−7.03	3	92	5

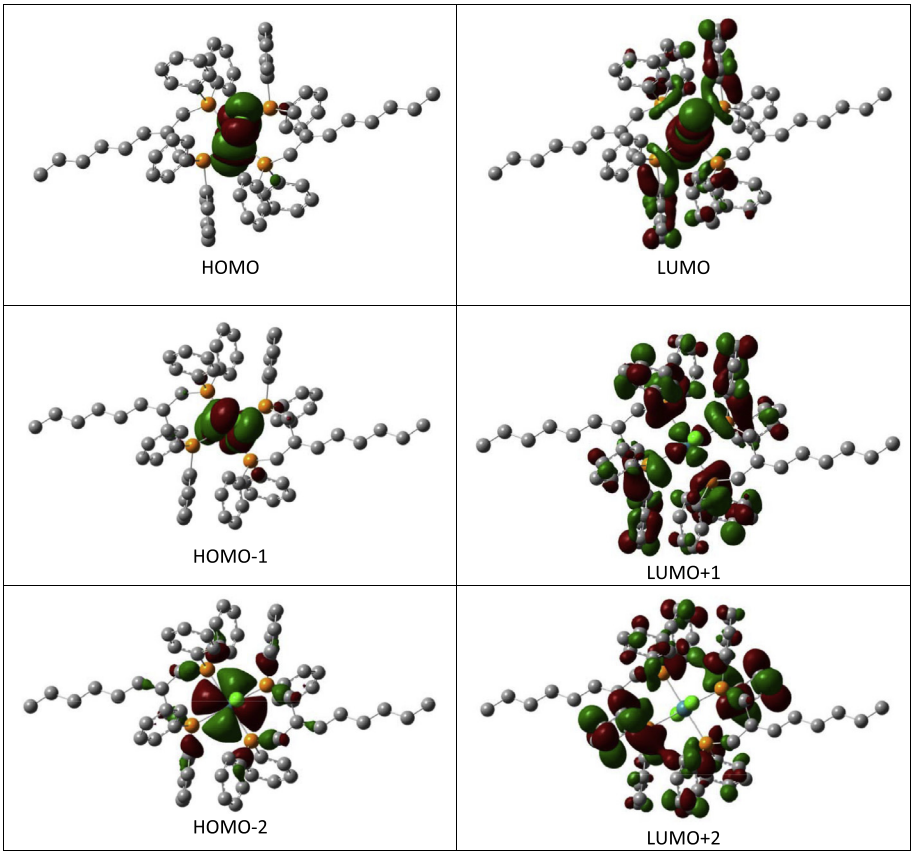

Fig. 5. Isodensity plots of the HOMO and LUMO orbitals of complex **1**.

Table 5
Computed excitation energies (nm), electronic transition configurations and oscillator strengths (*f*) for the optical transitions in the visible region of complex **1** and $\mathbf{1}^{+}$ transitions with $f \geqslant 0.006$ are listed).

Complex		*f*	Composition
1	306.0 (4.06)	0.0067	H−1 → L+4 (98%)
	303.7 (4.09)	0.0098	H → L+6 (96%)
	300.9 (4.13)	0.0105	H−1 → L+6 (95%)
	290.4 (4.28)	0.0154	H → L+8 (79%)
	288.9 (4.30)	0.0768	H−4 → L (38%), H−3 → L (37%)
	270.8 (4.59)	0.0223	H−4 → L+1 (18%), H−2 → L+2 (65%)
	268.8 (4.62)	0.205	H−3 → L+1 (35%), H−2 → L+2 (32%)
	266.9 (4.66)	0.3183	H−4 → L+1 (46%), H−3 → L+1 (43%)
$\mathbf{1}^{+}$	1056.6 (1.18)	0.0052	H−1(β) → L (β) (89%)
	761.4 (1.63)	0.0024	H−7(β) → L (β) (82%)
	726.7 (1.71)	0.0022	H−11(β) → L (β) (52%), H−8 (β) → L (β) (33%)
	661.7 (1.88)	0.0029	H−15 (β) → L (β) (76%)
	605.5 (2.05)	0.0034	H−19 (β) → L (β) (30%), H−18 (β) → L (β) (46%)
	585.4 (2.12)	0.0042	H−19 (β) → L (β) (54%), H−18 (β) → L (β) (36%)
	457.7 (2.71)	0.0039	H−30 (β) → L (β) (32%), H−23 (β) → L (β) (31%)
	444.9 (2.79)	0.0172	H (α) → L (α) (89%)
	433.1 (2.87)	0.028	H−1 (α) → L (α) (64%), H−24 (β) → L (β) (11%)
	402.6 (3.09)	0.0223	H (β) → L+1 (β) (81%)
	395.3 (3.14)	0.0884	H−1 (β) → L+1 (β) (72%)

in the high-energy side at 330 (≈269 and 266 nm (calculated)) nm which is resulted from two transitions, HOMO−3 → LUMO+1 (35%), HOMO−2 → LUMO+2 (32%) and HOMO−4 → LUMO+1 (46%), HOMO−3 → LUMO+1 (43%), is assigned to ligand–ligand charge transfer (Cl(pπ) →P(dπ)) charge transfer transitions [42].

Spectroelectrochemical study for complex **1** was performed in order to obtain the electronic absorption spectra of the complexes in their Ru(III) oxidation state (Fig. 6). The spectral transformations were reversible having greater than 90% recovery of the starting spectrum. Upon oxidation of **1**, the weak low energy d–d transition bands at 490–510 and 330–380 nm absorption band moving towards the ultraviolet (ca. 410 and 460 nm) and increasing in intensity. The intense high-energy band at 310 nm is shifted to lower energy and appears at 340 nm and a new a broad absorption band which appears at low energy and with an absorbance maximum at 704 nm.

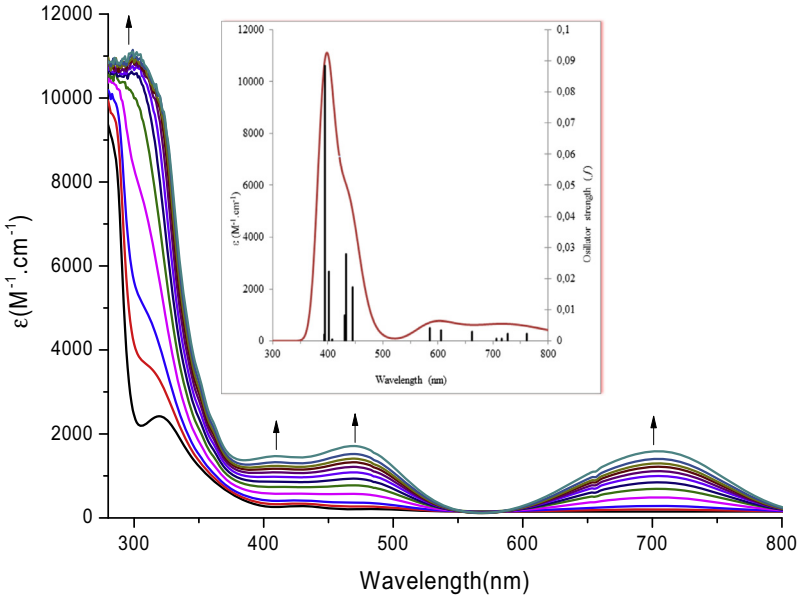

Fig. 6. Spectroelectrochemical experiment showing the absorption spectrum changes upon oxidation of a Dichloromethane solution of complex **1** and 0.1 M TBAH.

Theoretical calculations were performed on **1**$^{+}$**;** the calculations utilize both α and β occupied molecular orbitals. Relative percentages of atomic contributions to the lowest unoccupied and highest occupied molecular orbitals have been placed in Table 4. The Ruthenium (III) contributes to the HOMOs and in the range from LUMO/+1 with α spin and in the HOMO, HOMO−2 and LUMO/+1 with β spin. The Hdppp ligand contributes to LUMO+1 to LUMO+18 and HOMO−3 to HOMO−20 with α and β spin. TD-DFT calculations (Fig. 6) shows that the band centered at λ_{max} = 330 nm (≈395 nm (calculated)) resulted from H−1(β) which have sizable contributions of Hdppp and chloride ion to L+1 (β) which have sizable contributions of Hdppp and Ru(III). Thus this band is assigned to LLCT (ligand to ligand charge transfer). The two bands centered at 410 and 460 nm (≈433.1 and 444.9 nm (calculated)) reseluted from the overlap of several transitions, H(α) and H-1(α) which has a larger contribution of Hdppp to L (α) which has a larger contribution of Ru(III), thus this band is assigned to Hdppp (P(dπ)) → Ru(III) ligand-to-metal charge transfer (LMCT) transition. The low energy transition around 700 nm probably assigned to Chloride (pπ) → Ru(III) (dπ) LMCT transition.

4. Conclusions

Five neutral Ru(II) complexes with the formula *trans*-[Ru(P-P)$_2$Cl$_2$] (**1**–**5**) were prepared by reacting $RuCl_2(PPh_3)_3$ with P-P. Molecular structures of the complexes were determined by X-ray, and the spectroscopic properties were studied. The optimized structures were used for DFT calculations in order to determine the electronic properties of the complexes. The differences in the Ru(III/II) and the shift in the ^{31}P n.m.r. spectra are related to Ru(P-P) chelating ring and explain based on dft calculation. In the four-membered chelate complex the phosphorus resonates at lowest field and oxidized at lower potential, whereas the resonances of five-membered rings are observed at highest field and oxidized at higher potential. The signals of the phosphorous and Ru(III/II) of six-membered rings (**1**–**2**) are positioned in between these two extremer. The shift in the $E_{1/2}$ values for the *trans*-[Ru(P-P)$_2$Cl$_2$] (**1**–**5**) are related to the stability of the diphosphine complexes. The shielding and the chemical shift of the ^{31}P{1H} NMR is also related to Millikan charge for phosphorus atom which can be obtained from the dft theoretical calculation. Also, the more positively charged phosphorus atom the more deshielded it is. The absorption spectra of **1** and **1**$^{+}$ in dichloromethane were calculated with use of TD-DFT, and the transition characters were assigned using basis set, MWB/6-31+g(d,p) in connection with the molecular orbitals of the complexes.

Acknowledgements

Warad and M. Al-Noaimi would like to thank AN-Najah National University and The Hashemite University, Jordan for their research support.

Appendix A. Supplementary material

Crystallographic data have been deposited with the Cambridge Crystallographic Data Center, CCDC No. 782386 complex **1** and 714308 complex **3** Copies of this information may be obtained from the director, CCDC, 12 Union Road, Cambridge CB2 1EZ, UK. Tel.: +44 1223 762910; fax: +44 1223 336 033; e-mail: deposit@ccdc.cam.ac.uk or on the web http://www.ccdc.cam.ac.uk/deposit.

References

[1] C.C. Tai, J. Pitts, J.C. Linehan, A.D. Main, P. Munshi, P.G. Jessop, Inorg. Chem. 41 (2002) 1606.
[2] (a) I. Warad, E. Lindner, K. Eichele, H.A. Mayor, Inorg. Chim. Acta 357 (2004) 1847;
(b) E. Lindner, I. Warad, K. Eichele, H.A. Mayor, Inorg. Chim. Acta 350 (2003) 49;
(c) E. Lindner, H.A. Mayor, I. Warad, K. Eichele, J. Organomet. Chem. 665 (2003) 176.
[3] J. Chatt, R.G. Hayter, J. Chem. Soc. (1961) 896.
[4] J. Chatt, R.G. Hayter, J. Chem. Soc. (1961) 2605.
[5] (a) J.N. Anderson, N.J. Brookes, B.J. Coe, S.J. Coles, M.E. Light, M.B. Hursthouse, Acta Crystallogr., Sect. C 59 (2003) m215;
(b) S. Rigaut, J. Perruchon, L. Le Pichon, D. Touchard, P.H. Dixneuf, J. Organomet. Chem. 670 (2003) 37.
[6] T.A. Stephenson, G. Wilkinson, J. Inorg. Nucl. Chem. 28 (1966) 945.
[7] J.C. Briggs, C.A. McAuliffe, J. Chem. Soc., Dalton Trans. (1984) 423.
[8] M.M.T. Khan, R. Mohiuddin, Polyhedron 2 (1983) 1247.

[9] M. Al-Noaimi, M. Sunjuk, M. El-khateeb, S.F. Haddad, A. Haniyeh, Polyhedron 42 (2012) 66.
[10] M. Al-Noaimi, M.I. El-Barghouthi, O.S. Abdel-Rahman, S.F. Haddad, A. Rewashed, Polyhedron 30 (2011) 1884.
[11] M. Al-Noaimi, M. El-Barghouthi, M. El-khateeb, O. Abdel-Rahman, H. Goröls, R.J. Crutchley, Polyhedron 27 (12) (2008) 2698.
[12] E. Lindner, A. Enderle, A. Baumann, J. Organomet. Chem. 558 (1998) 235.
[13] I. Warad, M. Azam, U. Karama, S. Al-Resayes, A. Aouissi, B. Hammouti, J. Mol. Struct. 1002 (2011) 107.
[14] M. Krejcik, M. Danek, F. Hartl, J. Electroanal. Chem. 317 (1991) 179.
[15] C. Nataro, A.N. Campbell, M.A. Ferguson, C.D. Incarvito, A.L. Rheingold, J. Organomet. Chem. 673 (2003) 47.
[16] T. Gennett, D.F. Milner, M.J. Weaver, J. Phys. Chem. 89 (1985) 2787.
[17] Siemens, XSCANS. Siemens Analytical X-ray Instruments Inc., Madison, Wisconsin, USA, 1994.
[18] G.M. Sheldrick, Acta Crystallogr., Sect. A 64 (2008) 112.
[19] C.K. Johnson, ORTEPII. Report ORNL-5138, Oak Ridge National Laboratory, Tennessee, USA, 1976.
[20] C. Lee, W. Yang, R.G. Parr, Phys. Rev. B 37 (1988) 785.
[21] M.J. Frisch, G.W. Trucks, H.B. Schlegel, G.E. Scuseria, M.A. Robb, J.R. Cheeseman, J.A. Montgomery, Jr., T. Vreven, K.N. Kudin, J.C. Burant, J.M. Millam, S.S. Iyengar, J. Tomasi, V. Barone, B. Mennucci, M. Cossi, G. Scalmani, N. Rega, G.A. Petersson, H. Nakatsuji, M. Hada, M. Ehara, K. Toyota, R. Fukuda, J. Hasegawa, M. Ishida, T. Nakajima, Y. Honda, O. Kitao, H. Nakai, M. Klene, X. Li, J.E. Knox, H.P. Hratchian, J.B. Cross, V. Bakken, C. Adamo, J. Jaramillo, R. Gomperts, R.E. Stratmann, O. Yazyev, A.J. Austin, R. Cammi, C. Pomelli, J.W. Ochterski, P.Y. Ayala, K. Morokuma, G.A. Voth, P. Salvador, J.J. Dannenberg, V.G. Zakrzewski, S. Dapprich, A.D. Daniels, M.C. Strain, O. Farkas, D.K. Malick, A.D. Rabuck, K. Raghavachari, J.B. Foresman, J.V. Ortiz, Q. Cui, A.G. Baboul, S. Clifford, J. Cioslowski, B.B. Stefanov, G. Liu, A. Liashenko, P. Piskorz, I. Komaromi, R.L. Martin, D.J. Fox, T. Keith, M.A. Al-Laham, C.Y. Peng, A. Nanayakkara, M. Challacombe, P.M.W. Gill, B. Johnson, W. Chen, M.W. Wong, C. Gonzalez, J.A. Pople, GAUSSIAN 03 Revision D 01, GAUSSIAN Inc., Wallingford, CT, 2004.
[22] GaussView3.0, Gaussian, Pittsburgh, PA.
[23] P.J. Hay, W.R. Wadt, J. Chem. Phys. 82 (1985) 270.
[24] R. Bauernschmitt, R. Ahlrichs, Chem. Phys. Lett. 256 (1996) 454.
[25] M.K. Casida, C. Jamorski, K.C. Casida, D.R. Salahub, J. Chem. Phys. 108 (1998) 4439.
[26] R.E. Stratmann, G.E. Scuseria, M.J. Frisch, J. Chem. Phys. 109 (1998) 8218.
[27] M. Cossi, N. Rega, G. Scalmani, V. Barone, Comput. Chem. 24 (2003) 669.
[28] N.M. O'Boyle, A.L. Tenderholt, K.M. Langner, J. Comput. Chem. 29 (2008) 839.
[29] R. Mason, D.W. Meek, G.R. Scollary, Inorg. Chim. Acta 16 (1976) L11.
[30] S.O. Grim, W.L. Briggs, R.C. Barth, C.A. Tolman, J.P. Jesson, Inorg. Chem. 13 (1974) 1095.
[31] P.E. Garrou, Inorg. Chem. 14 (1975) 1435.
[32] G. Exarchos, S.D. Robinson, J.W. Steed, Polyhedron 19 (2000) 1511.
[33] A.A. Batista, C. Pereira, S.L. Queiroz, L.A.A. de Oliveira, R.H.D. Santos, M.T.D. Gambardella, Polyhedron 16 (1997) 927.
[34] A.R. Chakravarty, F.A. Cotton, W. Schwotzer, Inorg. Chim. Acta 84 (1984) 1979.
[35] M.R. Fontes, G. Oliva, L. Acácio, C. Cordeiro, A.A. Batista, J. Coord. Chem. 30 (1993) 125.
[36] T.S. Lobana, R. Singh, E.R.T. Tiekink, J. Coord. Chem. 21 (1990) 199.
[37] N. Camire, U.T. Mueller-Westerhoff, W.E. Geiger, J. Organomet. Chem. 637–639 (2001) 823.
[38] S. Lu, V.V. Strelets, M.F. Ryan, W.J. Pietro, A.B.P. Lever, Inorg. Chem. 35 (1996) 1013.
[39] B.K. Ghosh, A. Chakravorty, Coord. Chem. Rev. 95 (1989) 239.
[40] L.F. Szczepura, K.J. Takeuchi, Inorg. Chem. 29 (1990) 1772.
[41] S.I. Gorelsky, A.B.P. Lever, M. Ebadi, Coord. Chem. Rev. 230 (2002) 97.
[42] D.M. Massen, G.A. Crosby, J. Mol. Spectrosc. 25 (1968) 398.